PCCP

PAPER

Charge percolation in redox-active thin membrane hybrids of mesoporous silica and poly(viologens)†

Cite this: DOI: 10.1039/c8cp07192f

Simón Saint André, ‡[a] Federico Albanese,‡[a] Galo J. A. A. Soler-Illia *[bc] and Mario Tagliazucchi *[cd]

Received 22nd November 2018,
Accepted 8th January 2019

DOI: 10.1039/c8cp07192f

rsc.li/pccp

This work reports the fabrication of redox-active films of oligomeric and molecular viologens and mesoporous silica *via* the infiltration method. Pore-ellipsometry and UV-vis confirm that low-molecular-weight poly(viologens) in solution are able to enter the mesoporous structure, in contrast to high-molecular weight polymers that adsorb only on top of the film. Cyclic voltammetry shows that viologens are able to reach the bottom of the pores and access the electrode/film interface. However, the number of viologen sites that can be accessed by cyclic voltammetry at 50 mV s^{-1} is only a tenth of the total viologen population determined by UV-vis and pore-ellipsometry. The effect is ascribed to the very small apparent diffusion coefficient for charge transport within the film ($D_{app} < 10^{-12}$ cm^2 s^{-1}). A theoretical model is put forward to describe charge transport *via* the electron-hopping mechanism for redox sites randomly adsorbed on the inner walls of the pores. Our model predicts that the threshold of charge percolation occurs for viologen surface coverages close to those observed in our experiments; therefore, the low fraction of electrochemically addressable viologens is ascribed to inefficient charge percolation *via* the electron-hopping mechanism.

Introduction

Chemical modification of electrodes with molecular and polymeric thin films is a key technology for applications in amperometric (bio)sensors,[1,2] electrosynthesis,[3] electrochromic devices,[4–6] and corrosion protection.[7] In many examples of these applications, the thin film contains redox-active species, which are introduced by coordination, electrostatic binding or covalent attachment to the electrode surface or to previously deposited polyelectrolytes. For example, electrode surfaces can be modified by poly(vinylpiridine) and the pyridine units in the polymer can then be used to coordinate metal complexes.[8,9] Polyelectrolyte films on electrodes can also be used to incorporate redox-active counter ions *via* ion exchange,[10] for example Nafion® was used to bind redox cations, such as $Os(bpy)_3^{3+/2+}$ [11] and alkylviologens.[12]

Mesoporous inorganic materials are an interesting alternative to organic polymeric films for chemical modification of electrodes.[13] Depositing a mesoporous thin film onto a planar electrode introduces ion-permselective properties,[14,15] which are similar to those obtained by deposition of thin polyelectrolyte layers.[16–18] Like polymer thin films, mesoporous thin films can immobilize redox-active species. The advantages of redox-active mesoporous films over redox polymer films include improved mechanical properties and abrasion resistance, dimensional stability (*i.e.* absence of swelling) and a high degree of control over the nanometric composition and architecture of the system provided by the periodic arrangement of the pores in the inorganic scaffold. For example, Walcarius and coworkers reported the modification of mesoporous films *via* covalent attachment of ferrocene derivatives.[19,20] There are also reports of mesoporous silica materials modified by a viologen obtained *via* the co-condensation route.[21–23]

[a] *Departamento de Física, Facultad de Ciencias Exactas y Naturales, Universidad de Buenos Aires, Cuidad Universitaria, Buenos Aires 1428, Argentina*
[b] *DQIAQF, Facultad de Ciencias Exactas y Naturales, Universidad de Buenos Aires, Ciudad Universitaria, Pab. II, C1428EHA, Ciudad Autónoma de Buenos Aires, Argentina*
[c] *Instituto de Nanosistemas, Universidad Nacional de General San Martín, Av. 25 de Mayo y Francia, 1650, San Martín, Argentina. E-mail: gsoler-illia@unsam.edu.ar*
[d] *INQUIMAE, Facultad de Ciencias Exactas y Naturales, Universidad de Buenos Aires, Ciudad Universitaria, Pab. II, C1428EHA, Ciudad Autónoma de Buenos Aires, Argentina. E-mail: mario@qi.fcen.uba.ar*

† Electronic supplementary information (ESI) available: NMR spectra of PXV and PHV, CV measurements of the mesoporous silica film infiltrated with PXV adsorbed from a 0.5 M NaCl solution, the random sequential adsorption/charge percolation (RSA/CP) model, derivation of the equation to estimate the real surface coverage of molecules from experiments, simulation of 'split-wave' voltammograms, and estimation of the diffusion coefficient of charge transport within the film. See DOI: 10.1039/c8cp07192f

‡ These authors contributed equally.

The reports in the previous paragraph made use of covalent bonding to introduce the redox functionality into the films. Electrostatic adsorption is a simple and versatile alternative to covalent attachment. Chemically modified electrodes have been prepared by infiltration of molecular viologens into different types of zeolites and mesoporous materials.[24–28] Adsorption of non-redox polymers into mesopores has been reported by various groups[14,29–32] and the degree of infiltration into the pores has been shown to strongly depend on the molecular weight of the polyelectrolyte.[29,31,32] Caruso and collaborators explored adsorption of poly(acrylate) of different molecular weights (2–250 kDa) into amino-functionalized nanoporous silica with pore sizes in the range from 4 to 40 nm in solutions of different pH and ionic strength.[31] The authors show that long polymers cannot efficiently permeate into narrow pores and that, for low molecular weight polymers, the amount of adsorption decreased with increasing ionic strength. Brunsen and collaborators studied the adsorption of end-functionalized poly(vinylferrocene) onto mesoporous silica.[33] In this example, cyclic voltammetry did not reveal a signal due to ferrocene redox switching, and thus the authors concluded that the redox polymer was adsorbed on top of the mesoporous silica film rather than inside the pores. Stucky and coworkers prepared hybrid mesoporous titania/poly(3-hexyl thiophene) by spin coating the polymer onto the mesoporous film followed by a thermal treatment. The authors propose an even distribution of the polymer within the pores based on XPS results, although the electrochemical activity of the polymer was not addressed in that work.[34]

In this work, we demonstrate a hybrid material made of a mesoporous metal-oxide and an infiltrated redox polymer that exhibits electrochemical activity. More specifically, our material comprises oligomeric viologens electrostatically adsorbed into mesoporous silica films. We analyze these films with pore-ellipsometry, UV-vis spectroscopy, scanning electron microscopy, contact-angle measurements, cyclic voltammetry and electrochemical impedance spectroscopy. A main finding of our work is that only around a tenth of the redox molecules within the film are electrically addressable within the timescale of a slow-scan-rate cyclic voltammetry experiment (50 mV s^{-1}). We developed a charge percolation model to study electron-hopping for redox molecules adsorbed on the inner walls of cylindrical mesopores and show that charge transport is rather inefficient in this system due to its two-dimensional nature.

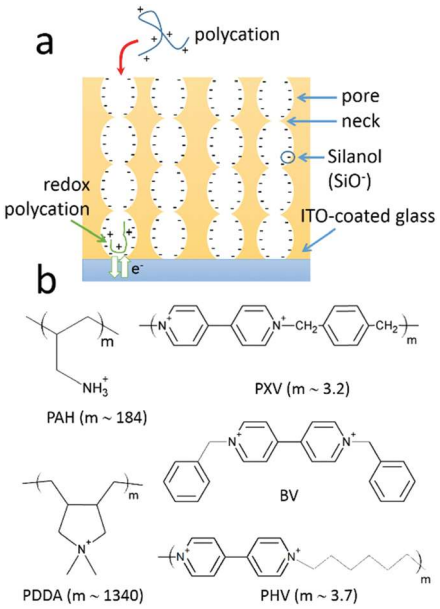

Fig. 1 (a) Scheme of the mesoporous silica film used in the adsorption studies. The typical thickness of the films is 140 nm and the diameters of the pore and the neck are 9 nm and 6 nm, respectively. (b) Chemical structures of the different molecules used in this work to infiltrate the mesoporous silica films.

Results and discussion

Characterization of mesoporous silica films

Fig. 1a shows a scheme of the mesoporous silica films. The top-view FE-SEM image of the film shown in Fig. 2a shows that the pores are arranged in a "4+2" pattern, compatible with an *Im*3*m* mesostructure, oriented with the [110] plane parallel to the surface.[35] We determined a cubic cell parameter of 20 ± 1 nm and an average pore radius, r_{pore}, of (4.2 ± 0.4) nm. Based on previous work, the pores are expected to have an ellipsoidal shape in the direction normal to the substrate due to uniaxial compression during the removal of the organic template; this contraction ensures the development of a continuous connectivity of the mesopore system.[36] We used ellipsoporosimetry to measure the ellipsometric quantities, ψ and Δ, as a function of the wavelength of the incident light, λ, and as a function of the relative humidity, P/P_0 (where P and P_0 are the vapor pressure of water in contact with the film and the saturation vapor pressure of water, respectively). By fitting the ellipsometric parameters with a single-layer model, *i.e.* a model that assumes that the film is a homogenous medium with an effective refractive index n_{eff}, we obtained the thickness of the film and $n_{eff}(\lambda)$ as a function of P/P_0 (see Fig. 2b). Typically, the thicknesses of our mesoporous films are between 140 and 150 nm. Increasing humidity leads to water adsorption, and eventually condensation into the pores. As water (refractive index n_{water} = 1.33) replaces air (n_{air} = 1.0), the effective refractive index of the film increases. Water adsorption–desorption curves exhibit two capillary condensation steps, and two superimposed hysteresis loops similar to type IV. This feature suggests that there are two mesopore systems with similar mesopore sizes, each of those behaving as a restricted system, *i.e.* presenting mesopores and openings that limit desorption and generate the hysteresis. Therefore, mesopore radii were estimated from the adsorption curve, and interpore necks were calculated from the desorption curve (Fig. 2c), using the analysis based on the Kelvin equation proposed by Boissiere *et al.*[37] Average radii of r = 4.5 ± 3.0 nm for the pores and r = 3.5 ± 0.5 nm for the necks were obtained, which are close to the pore sizes determined by SEM (4.2 ±

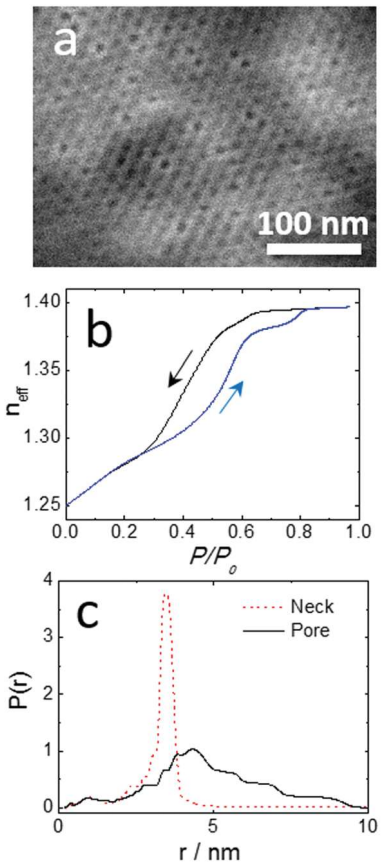

Fig. 2 (a) Top-view SEM image of the mesoporous film. (b) Typical plot of the effective refractive index of the film (n_{eff}) at 633 nm as a function of relative humidity, P/P_0. (c) Pore and neck radii distributions determined from the ellipsometric measurements.

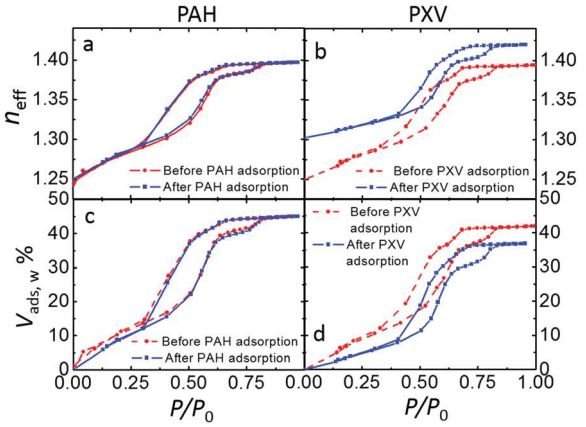

Fig. 3 (a and b) Effective refractive index of the mesoporous silica film (a and b) and water adsorption isotherms (c and d) as a function of the relative humidity before (red dashed line) and after (blue solid line) adsorption of PAH (a) or PXV (b) on the mesoporous silica films.

0.4 nm). The porosity of the films (30–44%) is of the same order of magnitude as the result of 20% estimated from the radius of the pore (using r_{pore} = 4.5 nm) and the separation between pores (19 nm, determined from the SEM images) using a simplified geometric model that considers cylindrical pores in a hexagonal array (see the ESI†).

Polyelectrolyte infiltration into mesoporous silica films

At pH > 2, the inner surface of the silica mesopores is negatively charged due to the acidity of the silanol groups; therefore one may expect that a polycation in solution can infiltrate the pores and adsorb onto their inner surfaces (see Fig. 1a). The main driving force for the adsorption of polyelectrolytes onto the inner surfaces of the pores is expected to be the release of the small counterions of the polyelectrolyte and the surface upon adsorption.[38] Previous reports in the literature[29,31,32] have shown that the molecular weight of the polyelectrolyte is critical in determining the amount of polyelectrolyte infiltrated into the pores. In preliminary ellipsometry experiments, we have observed that the polycations poly(allylamine) hydrochloride (PAH, M_w: 17 kDa) and poly(diallyldimethylammonium) chloride (PDDA, M_w: approx. 100 kDa) do not significantly affect either the refractive index of the dry film or its dependence with ambient humidity, see for example Fig. 3a for PAH adsorption. We conclude that under the conditions explored, relatively long-chain PAH and PDDA are unable to adsorb into the pores of our mesoporous silica films due to their large molecular weight.[29,31]

Since high-molecular-weight polyelectrolytes were unable to enter the pores, we prepared and used low-molecular-weight (M_w approx. 1 kDa) viologen oligomers obtained *via* the co-condensation synthetic route[39,40] to explore the preparation of redox-active mesoporous films *via* the infiltration method. Fig. 3b shows n_{eff} *vs.* humidity curves for mesoporous films infiltrated with poly(xylyl viologen), PXV (see the structure in Fig. 1b). We observed a significant increase in the refractive index for all humidities, indicating that PXV was successfully adsorbed into the pores. This result is supported by the analysis of the water adsorption isotherm, which shows a marked decrease in the maximum amount of adsorbed water upon PXV adsorption (Fig. 3d, compare with Fig. 3c for PAH).

From the values of the refractive index of the film, n_{eff}, we calculated the porosity of the film and the volume fraction of the pores filled by the polymer using the Bruggeman effective medium model. In the absence of the polymer, the Bruggeman effective medium model is given by:

$$p\left[\frac{n_{air}^2-n_{eff}^2}{n_{air}^2+2n_{eff}^2}\right]+(1-p)\left[\frac{n_{Si}^2-n_{eff}^2}{n_{Si}^2+2n_{eff}^2}\right]=0 \qquad (1)$$

where p is the porosity of the film (volume fraction of the film occupied by pores), and n_i is the refractive index of species i (i = air, pol and Si for air, polymer and silica, respectively). We determined p for each film before the adsorption of viologen oligomers from the n_{eff} values at P/P_0 = 0% using n_{air} = 1 and n_{Si} = 1.455. Using the resulting values of p, we then obtained the volume fraction of the pores that is occupied by the oligoviologens, ϕ_{pol}, using the refractive index of the sample after PXV adsorption and the Brugemann effective medium model for a

Table 1 Film porosity (p), volume fraction of the pore occupied by polycations (ϕ_{pol}), ellipsometrically determined surface coverage of the polycations (Γ_{ell}) and contact angle of the film before (θ_0) and after (θ_{ads}) adsorption of the polycations for mesoporous silica films infiltrated with different polycations. The batch number (B.N.) indicate the synthetic batch of the silica films, which show some variability in their porosities

B.N.	Species	p (%)	ϕ_{pol} (%)	Γ_{ell}/nmol cm^{-2}	θ_0/°	θ_{ads}/°
1	PAH	44	0	0	22 ± 5	41 ± 5
1	PXV	42	27	5.3	20 ± 5	36 ± 5
1	PXV + 0.5 M NaCl	40	44	8.2	21 ± 5	33 ± 5
2	PXV	31	28	4.0	23 ± 5	32 ± 5
2	BV	30	21	2.4	22 ± 5	44 ± 5

system containing air, viologens and silica:

$$p\left(1-\phi_{pol}\right)\left[\frac{n_{air}^2-n_{eff}^2}{n_{air}^2+2n_{eff}^2}\right]+p\phi_{pol}\left[\frac{n_{pol}^2-n_{eff}^2}{n_{pol}^2+2n_{eff}^2}\right]+(1-p)\left[\frac{n_{Si}^2-n_{eff}^2}{n_{Si}^2+2n_{eff}^2}\right] \quad (2)$$

where n_{pol} is the refractive index of the viologen oligomers (we used n_{pol} = 1.45[41]). The values of p and ϕ_{pol} for different experiments are compiled in Table 1. Note that the table contains information for two different synthetic batches of the silica mesoporous film, which show some inter-batch variations of porosity. The value of ϕ_{pol} allows us to obtain an ellipsometry-based estimation of the surface coverage of the viologen (moles of viologen monomers per unit area of the substrate), Γ_{ell}, using the formula:

$$\Gamma_{ell}=\frac{p\phi_{pol}\delta\rho_{pol}}{M_m} \quad (3)$$

where δ is the thickness of the mesoporous film (determined by ellipsometry), ρ_{pol} is the density of the dry oligoviologens (we used ρ_{pol} = 1.1 g mol^{-1}) and M_m is the molecular weight of the monomer.

Table 1 shows that 27–28% of the volume of the pores becomes filled with PXV upon adsorption. Adding 0.5 M of NaCl to the PXV solution increases this fraction to 44%. Note that the amount of polyelectrolyte adsorbed on a charged surface can decrease or increase with added salt because increasing ionic strength plays the dual role of screening polyelectrolyte–surface attractions (which favor adsorption) and polyelectrolyte–polyelectrolyte repulsions (which hinder adsorption).[42] In Table 1 we also report experiments performed with benzyl viologen (BV^{2+}, see the structure in Fig. 2b), which is a small molecule similar to the monomeric unit of PXV.

Table 1 shows the contact angle of the samples before and after adsorption. It is interesting to note that the adsorption of the high-molecular-weight polyelectrolytes (PAH and PDDA) affects the contact angle of the surface, which suggests that even while these polyelectrolytes cannot infiltrate into the pores, they can still form a very thin layer of a few nanometers on the outer surface of the silica film. This ultrathin layer could not be measured by ellipsometry, but it affects the wetting properties.

Estimation of the total surface density of viologens by UV-vis spectroscopy of chemically reduced samples

In order to provide an alternative to ellipsometry for the estimation of the amount of adsorbed viologens, we performed spectroscopic quantification of the chemically reduced samples.[39] We chemically reduced the viologens adsorbed within the mesoporous films by immersing the samples in 10 mM $Na_2S_2O_4$ solution under an Ar inert atmosphere. The UV-vis spectra of the reduced samples (Fig. 4) show a broad absorption band between 500 and 700 nm, which is characteristic of the viologen radical cation.[39,43] In the case of BV, this broad band is composed of two convoluted bands at 550 and 600 nm, which were assigned to the monomer and dimer of the BV radical cation.[44] The intensity of this band allows for a spectrophotometric estimation of the amount of viologen units present in the film per unit area of the substrate, using the formula $\Gamma_s = A/\varepsilon$, where A is the peak absorption and ε is the extinction coefficient (we used $\varepsilon = 1.2 \times 10^7$ cm^2 mol^{-1} = 1.2×10^4 M^{-1} cm^{-1} [43,44]). Table 2 compares the surface coverages determined by ellipsometry (Γ_{ell}) and UV-vis spectroscopy of reduced viologens (Γ_{abs}). The trends of Γ_{ell} observed in Table 1 for experiments with added salt and adsorption of BV are also observed for Γ_{abs}, however the values of Γ_{ell} are systematically higher than those of Γ_{abs} by factors between 2.1 and 3.7. In the UV-vis absorption method, the absorption of the sample is linearly proportional to the surface coverage of the viologens, and the value of the proportionality constant (*i.e.* the extinction coefficient) is well known from the literature;[43,44] therefore the spectroscopic method provides a very straightforward measurement of the surface coverage. While desorption of reduced viologens from the pores in the spectroscopic method can result in an underestimation of the surface coverage of

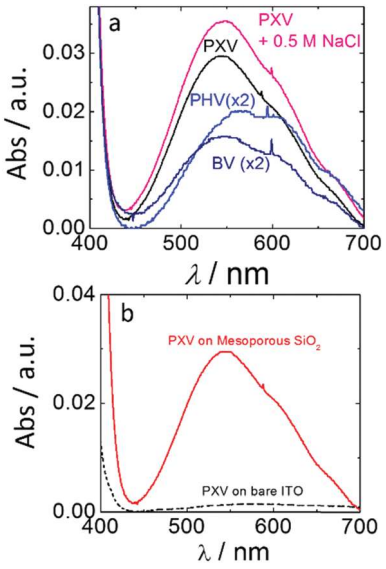

Fig. 4 (a) UV-vis spectra of chemically reduced viologens adsorbed into mesoporous silica films. (b) Comparison of the spectra of chemically reduced PXV adsorbed on a mesoporous silica film and adsorbed on bare ITO-coated glass.

Table 2 Comparison of the surface coverage (molecules per geometric area of the electrode) determined by ellipsometry (Γ_{ell}), UV-vis spectroscopy of chemically reduced samples (Γ_{abs}) and cyclic voltammetry (Γ_{CV}) and the fraction of electrochemically addressable sites, Γ_{CV}/Γ_{abs}, for different viologen species and added salt (C_{salt}). N.M.: not measured

Viologen	C_{salt} (M)	Γ_{ell}/nmol cm^{-2}	Γ_{abs}/nmol cm^{-2}	Γ_{CV}/nmol cm^{-2}	Γ_{CV}/Γ_{abs}
PXV	0	5.3	2.5	0.20	0.08
PXV	0.5	8.2	2.9	0.11	0.038
BV	0	2.4	0.65	0.098	0.15
PHV	0	N.M.	0.83	0.087	0.10

viologens, this error is unlikely because the electrochemical experiments discussed below showed almost no decrease of the charge of the viologen^{2+}/viologen^{1+} peak with the number of potential cycles. On the other hand, the ellipsometric determination of the surface coverage is less direct and more susceptible to errors than the UV-vis absorption method because (i) the relationship between Γ_{ell} and n_{eff} is complex and depends on the refractive index and density of the polymer, for which we used educated guesses, and (ii) Γ_{ell} strongly depends on the porosity of the film, for example for the PXV experiment in Table 2, a decrease of only 20% in the porosity (from 42% to 33.6%) would cause a decrease of Γ_{ell} by a factor of 5 (from 5.3 to 1.08 mol cm^{-2}). It should also be mentioned that we used ITO substrates for UV-vis and silicon substrates for ellipsometry. The substrate can affect the ordering of the mesopores in the film, thus affecting the adsorption of the viologen. In summary, we believe than the estimation of surface coverage by UV-vis is less prone to errors than the ellipsometric method.

Determination of the surface coverage of electrochemically addressable viologens by cyclic voltammetry (CV)

We used cyclic voltammetry to study the electrochemical response of mesoporous silica infiltrated by different viologen species. In addition to poly(xylyl viologen) (PXV), we studied poly(hexyl viologen) (PHV, an oligomeric viologen with a similar degree of polymerization to PXV) and benzyl viologen (BV, a molecular viologen). The structures of all viologens used in this work are shown in Fig. 1b. Fig. 5 shows cyclic voltammperograms using a scan rate of 50 mV s^{-1} for ITO-on-glass electrodes coated by mesoporous silica films before and after adsorption of PXV (Fig. 5a), BV (Fig. 5b) and PHV (Fig. 5c) under an Ar atmosphere. We also measured the cyclic voltammperogram for PXV adsorbed from a NaCl 0.5 M solution, which is similar to the one in in Fig. 5a and is reported in the ESI† (Fig. S3). All voltammperograms (both before and after adsorption) show a cathodic catalytic wave at electrode potentials more negative than −0.7 V due to oxygen reduction at the ITO electrode.[5] The PHV sample (Fig. 2c) reproducibly shows one oxidation peak and two reduction peaks. The anodic (oxidation) peak at −0.56 V and the cathodic (reduction) peak at −0.63 V are assigned to the viologen^{2+}/viologen^{1+} redox couple.[5,45] The cathodic peak at −0.5 V originates from the reduction of oxygen mediated by reduced viologens[46] (we were unable to eliminate this peak even after thoroughly bubbling the electrolyte

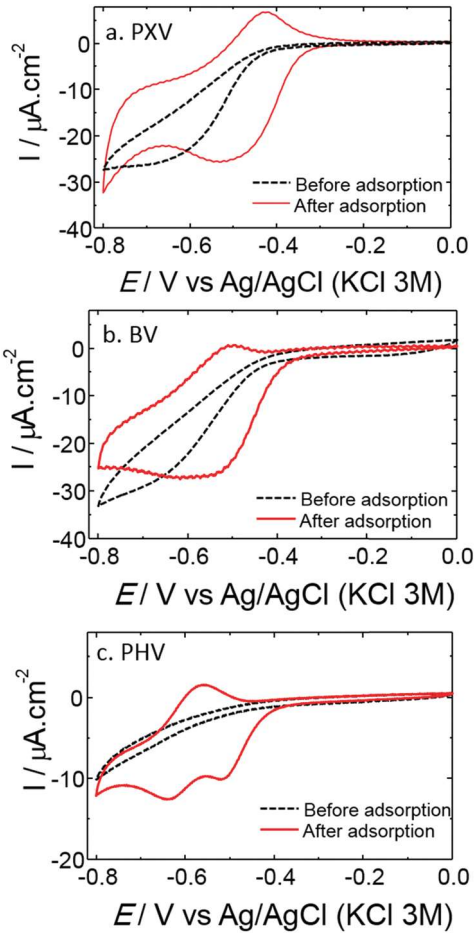

Fig. 5 (a) Cyclic voltamperograms of mesoporous silica films on ITO-coated glass before and after adsorption of PXV (a), BV (b) and PHV (c) under an Ar atmosphere and in 50 mM KNO_3 electrolyte. Scan rate: 50 mV s^{-1}.

solution with Ar). The characteristic waveshape of the cyclic voltammogram in Fig. 5c ('split wave' voltamperogram[46]) is a consequence of the very fast reduction of oxygen by the viologen radicals combined with the fact that the formal reduction potential for oxygen reduction to superoxide (−0.38 V *vs.* Ag/AgCl[47]) is more positive than that of the viologen/viologen radical couple.[46] Under these conditions, the reduction of oxygen starts at potentials more positive than the formal potential of the mediator, which produces a cathodic catalytic peak as oxygen near the electrode becomes depleted. In the case of PXV (Fig. 5a) and BV (Fig. 5b), the catalytic oxygen reduction peak is also present, but overlaps with the viologen reduction peak, which produces a single broad cathodic peak. The fact that the oxygen-reduction and viologen-reduction peaks overlap for PXV and BV but not for PHV is ascribed to the fact that PHV has a more negative reduction potential than PXV and BV (see potentials of the anodic peaks in Fig. 5).

In order to determine the number of viologen sites that can be addressed in the time scale of the experiment, we integrated the anodic peak for each of the voltammperograms in Fig. 5. At this point, it is important to assess the potential interference of

catalytic reduction of oxygen in the electrochemical determination of the viologen surface coverage (note that this interference was minimized by conducting the CV experiments under an inert atmosphere, but we were unable to remove it even after thoroughly bubbling the solutions with Ar). In principle, we expect that the error in the determination of the surface coverage by integration of the anodic peak will be small because oxygen near the film is almost depleted during the cathodic scan and, due to its low concentration in solution, its diffusional flux is very small. We validated the use of the integrated charge of the anodic peak to obtain the number of electrochemically addressable viologen sites in the electrode by simulating cyclic voltammperograms of an electrode modified by a viologen film in the presence of oxygen with the model of Compton and coworkers[46] for the catalytic reduction of oxygen by viologen (see the ESI†). Using the simulated cyclic voltammograms, we observed that the integrated charge of the anodic peak, Q/A, may underestimate the surface coverage of viologens ($\Gamma_{CV} = (Q/A)/F$, where F is Faraday's constant), but the error is always smaller than 20%. We therefore determined the experimental integrated charge per unit area of the electrode of the anodic peaks to estimate Γ_{CV} for the different viologens under study and report them in Table 2.

It is noteworthy that the values of Γ_{CV} in Table 2 are around one order of magnitude smaller than the surface coverages measured by UV-vis spectroscopy, Γ_{abs}. In other words, only around one tenth of the viologen sites present in the film can be electrochemically reduced/oxidized on the timescale of the CV experiment. As we discussed in the last paragraph, this difference is much larger than the error introduced by estimating the surface coverage from the integrated charge in the CV.

Discussion of the origin of the low fraction of viologen sites that are addressable by CV

We hypothesise that the low fraction of viologen sites detected by low-scan-rate CV experiments is due to inefficient diffusional charge transport within the film. The cyclic voltammperograms in Fig. 5 show in fact peak separations of 101 mV (PXV), 62 mV (BV) and 74 mV (PHV), which are close to the ideal value of 58 mV for a diffusion-controlled process.[48] In principle, it should be possible to increase the fraction of addressable sites by reducing the scan rate of the CV experiment, and obtain an apparent electron-hopping diffusion coefficient, D_{app}, from the dependence of the CV shape on the scan rate.[49] Unfortunately, the interference of oxygen reduction becomes more relevant as the scan rate decreases. Therefore, we used electrochemical impedance spectroscopy (EIS) to probe charge transport in a film infiltrated with PXV. We set the electrode potential for the EIS experiment at the redox potential of the PXV couple, −0.5 V. At this potential, oxygen should get rapidly depleted from the electrode surface, therefore we analyzed the impedance spectrum of the system using an equivalent circuit for redox-modified electrodes in the absence of electrocatalysis.[50,51] The equivalent circuit (shown as an inset in Fig. 6) comprises a solution resistance R_s in series with a parallel combination of the double layer capacitance C_{dl} (which we model as a constant phase element) on one branch and a series combination of the

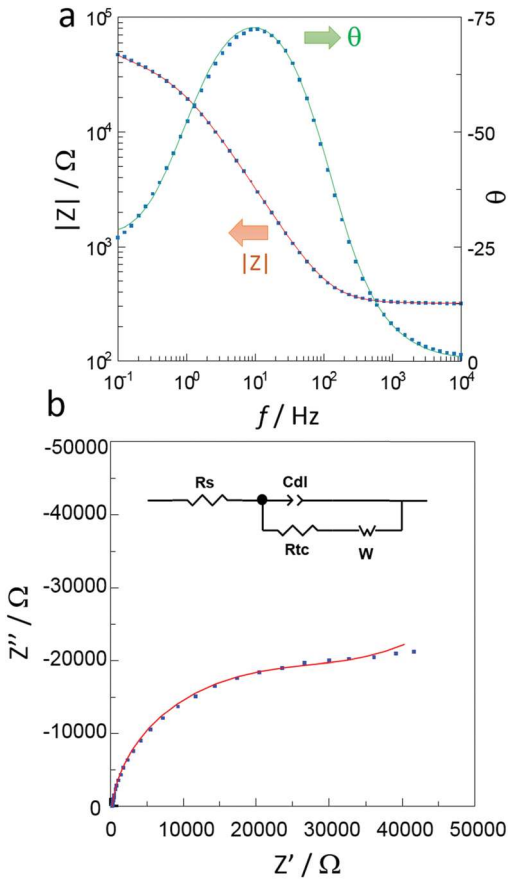

Fig. 6 Bode (a) and Nyquist (b) plots of the electrochemical impedance spectrum of a PXV-modified silica film on ITO-coated glass at $E = -0.5$ V, under an Ar atmosphere and in 50 mM KNO_3 electrolyte. Solid lines show the best fit with the equivalent circuit in the inset of panel b.

charge-transfer resistance (R_{ct}) and a bound-diffusion Warburg element (W) on the other. The impedance of the Warburg element depends on the total surface coverage of redox sites (Γ_{EIS}) and the apparent diffusion coefficient for charge transport, D_{app}.[50] We obtained a good fitting of the EIS data (solid lines in Fig. 6) using $D_{app} = 4.1 \times 10^{-13}$ cm^2 s^{-1}, $\Gamma_{EIS} = 2.0$ nmol cm^{-2}, $R_s = 79.2$ Ω cm^2, $R_{ct} = 8.0$ kΩ cm^2 and $C_{dl} = 28$ μF cm^{-2} Hz^{1-n} (where $n = 0.93$ is the best fit value for the exponent of the constant phase element). Comparison with Table 2 shows that Γ_{EIS} is closer to Γ_{abs} (2.5 nmol cm^{-2}) than to Γ_{CV} (0.2 nmol cm^{-2}), which supports our results because Γ_{EIS} is the total surface coverage, while Γ_{CV} is the surface coverage that can be electrochemically addressed in a CV experiment at $v = 50$ mV s^{-1}.

As an alternative method to estimate the value of D_{app}, we simulated cyclic voltammograms explicitly considering charge transport in the film[49] at 50 mV s^{-1} as a function of D_{app} (see the ESI†). We then integrated the peaks of the simulated cyclic voltammograms and determined the values of D_{app} that yielded the fractions of electrochemically active viologen sites reported in Table 2 (Γ_{CV}/Γ_{abs}). This analysis resulted in values of D_{app} between 8×10^{-14} (for $\Gamma_{CV}/\Gamma_{abs} = 0.038$) and 1.2×10^{-12} cm^2 s^{-1} (for $\Gamma_{CV}/\Gamma_{abs} = 0.15$). These values are consistent with that

obtaind from the EIS experiment in Fig. 6 ($D_{app} = 4.1 \times 10^{-13}$ cm^2 s^{-1}). A value of $D_{app} < 1.2 \times 10^{-12}$ cm^2 s^{-1} is very small compared with the values of D_{app} typically observed in films of redox polymers, which are on the order of 10^{-8}–10^{-10} cm^2 s^{-1}.[49,50,52–54] This analysis suggests that inefficient diffusional charge transport is the origin of the low fraction of viologen sites that are addressable during low-scan rate cyclic voltammetry experiments.

Inefficient charge transport within the film can be ascribed either to slow electron-hopping or to slow diffusion of counter-ions (which are required to balance the charges created during the redox process[55]). We did not observe an increase in the redox charge of the film in CV experiments upon increasing the ionic strength of the measuring solution from 50 mM to 1 M, thus we believe that inefficient charge transport is not due to slow counter ion diffusion.

An alternative explanation for the low fraction of electrochemically addressable viologens observed in Table 2 is that some sites cannot be reached by electron-hopping at all and thus they cannot be electrically addressed independently of the time scale of the experiment. For example, it is possible that oligoviologens adsorb first on the pore openings, thus preventing further diffusion into the pores due to steric or electrostatic repulsion. Based on our experiments, we believe, however, that these mechanisms cannot completely explain the observed effect. If steric hindrance is responsible for the low fraction of electrochemically addressable molecules, then this fraction should substantially increase when using molecular viologens instead of oligoviologens. However, the fraction of electrochemically addressable viologens (*i.e.* Γ_{CV}/Γ_{abs}, see Table 2) for BV is 0.15, which is still far from unity and only slightly larger than those for PXV (0.080) and PHV (0.10). On the other hand, electrostatic hindrance to viologen diffusion should be eliminated by performing the adsorption from high ionic-strength conditions; however we observe that adding 0.5 M NaCl to the PXV solution does not increase the fraction of electrochemically addressable viologens (0.080 for no added NaCl and 0.038 for 0.5 M added NaCl). It is also possible that some of the pores will be blocked and not even connected to the electrode (*i.e.* 'dead ends'), but the fraction of this type of pores will be definitely small since previous experiments have shown that redox probes in solution can permeate through the pores and efficiently access the underlying electrode.[14,15]

In summary, we observe that CV at 50 mV s^{-1} can only access around a tenth of the viologen sites in the film and ascribe this limitation to inefficient electron hopping in the film. A relevant question is how the effect of confining the viologens to the inner surface of the nanopores can affect electron-hopping, compared to a homogenous spatial distribution of redox sites (which is expected, for example, for redox polymer-modified electrodes). To further analyse this effect, we propose a simple charge-percolation model inspired by redox-active polymers, which is presented below.

Simulation of charge transport between redox centers adsorbed in mesoporous films

In charge transport *via* the electron-hopping mechanism[50,56] the electrochemical reaction is propagated through the film by successive electron-transfer events ("hopping") between redox sites in different oxidation states. Electron hopping is efficient in redox-polymer films,[45,49,50,56] where the sites are homogenously distributed in space and the segmental motions of the polymer assist electron-transfer events.[57] On the other hand, molecules adsorbed in mesoporous films are located only on the inner surfaces of the pores, and, therefore, diffusion occurs on an effectively two-dimensional system. In order to explore charge percolation for fixed sites on the inner surface of a pore, we propose a simple random-sequential-adsorption/charge-percolation (RSA/CP) model, which is summarized in Fig. 7a.

To formulate the RSA/CP model, let us first define Γ^{real} as the surface density of redox molecules irreversibly adsorbed on the inner surface of a cylindrical pore, where the superscript real indicates that the surface density is expressed in terms of the real area of the mesoporous film rather than the geometric area of the electrode, as was used for the Γ values reported in Table 2. For a given value of Γ^{real}, we first determine the number of molecules per pore of radius r_{pore} and length l_{pore}. The molecules are placed on the cylinder using a random-sequential adsorption (RSA) algorithm.[58,59] In other words, for each molecule we first randomly select an adsorption position on the inner surface of the pore. We place the molecule at that

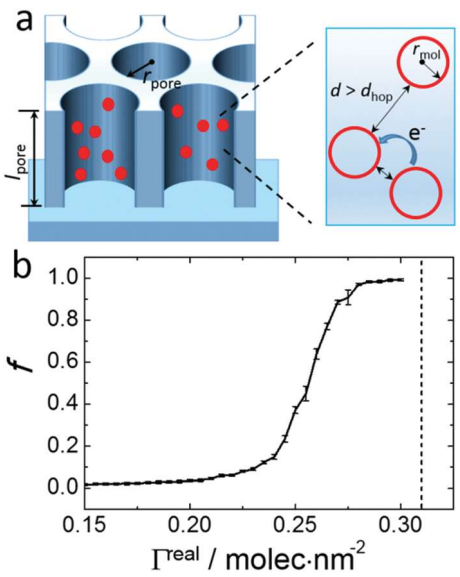

Fig. 7 (a) Scheme showing the parameters of the random sequential adsorption/charge percolation model. We assume cylindrical pores of radius r_{pore} and length l_{pore}. Molecules are adsorbed *via* a random sequential adsorption mechanism on the inner surface of the pores up to a surface density Γ^{real}. In this process, we do not allow the centers of the molecules to be placed at a distance smaller than one molecular diameter, $2{\cdot}r_{mol}$. Charge percolation in the system follows an electron-hopping mechanism, where electrons hop between two molecules if their separation is smaller than the hopping range, d_{hop}. (b) Average fraction of electrochemically addressable redox sites as a function of Γ^{real} for r_{pore} = 4.5 nm, l_{pore} = 140 nm, r_{mol} = 0.75 nm and d_{hop} = 0.5 nm. Error bars indicate one standard deviation of f obtained from 200 independent calculations for each point. The vertical dashed line indicates the maximum surface coverage achievable *via* random sequential adsorption for the parameters of the calculation.

position only if it does not overlap with any of the previously adsorbed molecules (*i.e.* the distances between the center of the molecule being adsorbed and the centers of all previously adsorbed molecules should be larger than one molecular diameter, $2{\cdot}r_{mol}$). We repeat this process until the desired number of molecules has been adsorbed. We then determined the fraction of molecules that are actually connected to the electrode using a charge-percolation (CP) algorithm (see the ESI†). In the CP algorithm, electron hopping between two molecules occurs only if they are located at a distance d_{hop} or smaller.

For each set of conditions, we performed 200 independent repetitions with the RSA/CP model and report an average value of the fraction of electrochemically addressable molecules in the pore, f. Fig. 7b shows f *vs.* Γ^{real} for a set of parameters which roughly model the dimensions of the experimental pores and the BV molecules, and a hopping range d_{hop} = 0.5 nm. The vertical dashed line indicates the maximum surface density achievable *via* RSA. This surface density was estimated from the maximum packing density (ratio of the area occupied by disks to the total area) for RSA of hard disks on a planar surface of 54.7%.[58] This packing efficiency is much smaller than the maximum packing efficiency for hard disks (90.7% for hexagonal packing) due to jamming of the molecules during RSA. In the conditions of Fig. 7b, we find a sharp percolation transition around Γ^{real} = 0.25 molec nm^{-2}.

Table 3 shows the values of Γ^{real} determined from the experimental surface coverages. In order to determine Γ^{real}, we assumed again cylindrical pores, which results in the following equation (derived in the ESI†):

$$\Gamma^{real} = \frac{r_{pore} \cdot \Gamma}{l_{pore} \cdot p} \quad (4)$$

where r_{pore} = 4.5 nm, l_{pore} = 140 nm, p is the porosity of the film obtained from ellipsometry (40%) and Γ is the experimentally determined surface coverage in terms of the geometric area of the electrode (values in Table 2). The value of Γ^{real} determined from UV-vis for BV is 0.16 molec nm^{-2}, which is slightly smaller than the theoretical percolation threshold estimated for BV (0.25 molec nm^{-2}). This result supports inefficient charge transport *via* electron-hopping being the cause of the low fraction of viologen sites measured in the CV experiment.

Fig. 8 shows the results of a systematic analysis of the effect of the different variables involved in the RSA/CP model. Fig. 8a shows that increasing the size of the molecules (r_{mol}) decreases the threshold value of Γ^{real} for percolation because the minimum center-to-center distance required for electron hopping is equal to the molecular diameter plus the hopping distance, d_{hop}, see Fig. 8a; therefore, increasing the maximum center-to-center hopping distance decreases the percolation threshold. Interestingly, for sufficiently large molecules (*e.g.* $r_{mol} > 2$ nm for the parameters in Fig. 8a), the maximum surface density achievable by RSA (vertical dashed lines) is smaller than the percolation threshold and, therefore, charge percolation becomes impossible in all conditions. Fig. 8b analyzes the effect of the hopping range and shows that, as expected, the

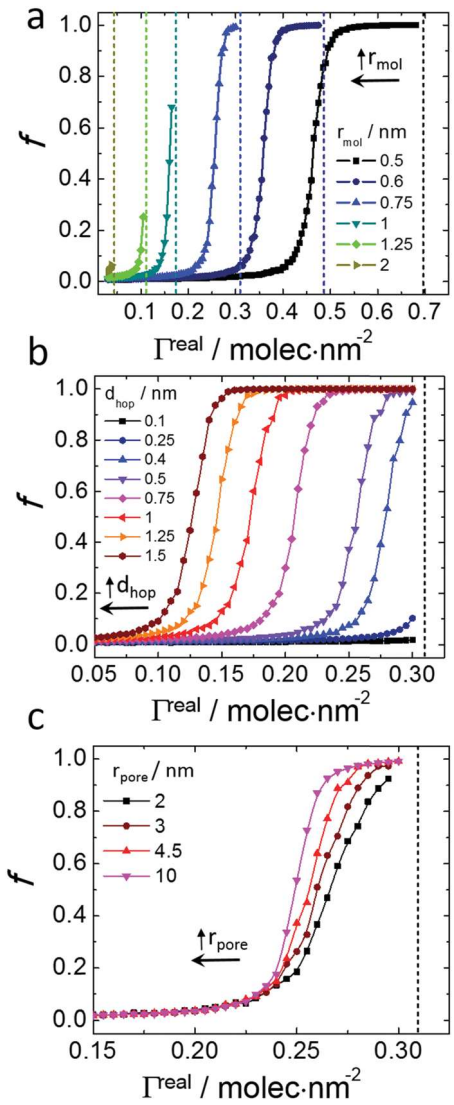

Fig. 8 Effect of the radius of the molecule (r_{mol}, panel a), electron-hopping range (d_{hop}, panel b) and pore radius (r_{pore}, panel c) on the fraction of electrochemically addressable redox sites (f) as a function of the surface density of redox molecules on the surface of the pore (Γ^{real}), calculated with the random sequential adsorption/charge percolation model. Calculation parameters: r_{pore} = 4.5 nm (except panel c), l_{pore} = 140 nm, r_{mol} = 0.75 nm (except panel a) and d_{hop} = 0.5 nm (except panel b). The vertical dashed lines in each plot indicate the maximum surface coverages achievable *via* random sequential adsorption.

Table 3 Real surface coverage (molecules per unit area of the inner surface of the pore) estimated for different viologen species and added salt (C_{salt}) using the results in Table 2 and assuming that the film comprises an array of cylindrical pores with a radius of 4.5 nm, length of 140 nm and an overall porosity of 40%. N.M.: not measured

Viologen	C_{salt} (M)	Γ_{ell}^{real}/ molec nm^{-2}	Γ_{abs}^{real}/molec nm^{-2}	Γ_{CV}^{real}/molec nm^{-2}
PXV	0	1.3	0.60	0.048
PXV	0.5	2.0	0.70	0.027
BV	0	0.58	0.16	0.024
PHV	0	N.M.	0.20	0.021

percolation threshold decreases as the hopping range, d_{hop}, increases. For small enough hopping ranges ($d_{hop} < 0.25$ nm for the conditions of Fig. 8b), the maximum RSA packing density is smaller than the percolation threshold and thus percolation becomes impossible. Fig. 8c shows that the percolation threshold increases as the pores become narrower. The average number of molecules located at a given distance from the electrode scales linearly with the perimeter of the pore and thus with its radius. Increasing the number of molecules at a given distance from the surface increases the number of possible percolation pathways; therefore, it facilitates charge propagation in the direction normal to the electrode and lowers the percolation threshold.

We finally compared charge percolation in the pore against a homogeneous film of the same thickness (140 nm). In the case of the homogeneous film, we allowed the sites to be located in any position within the calculation box and used periodic boundary conditions in the x–y directions. The percolation threshold for the case of viologens adsorbed into cylindrical nanopores (example in Fig. 7b) occurs for $\Gamma^{real} = 0.25$ molec nm^{-2}, which corresponds to an average intermolecular distance of $(\Gamma^{real})^{-1/2} = 2$ nm. As a comparison, a homogeneous film (for $r_{mol} = 0.75$ nm and $d_{hop} = 0.5$ nm, same conditions as in Fig. 7b) shows a percolation threshold for a concentration of redox sites $c = 0.09$ molec nm^{-3}, which corresponds to an average intermolecular distance of $c^{-1/3} = 2.2$ nm. Therefore, charge percolation is more efficient for homogeneously distributed redox sites than for pore-confined redox molecules.

As a conclusion, our analysis supports the finding that inefficient electron hopping is the main cause of the low fraction of electrochemically addressable molecules in the CV experiment. Our theoretical model also indicates that nanoconfinement of the redox sites to the inner surface of a nanopore decreases the efficiency of charge transport compared to homogeneously distributed redox sites. The RSA/CP model is, of course, very approximate and serves only as a first theoretical approach to the problem of charge transport *via* electron-hopping in a nanoconfined geometry. We resort to several assumptions, such as using a cylindrical shape for the pore, neglecting the shape of the molecule and using an educated guess for the hopping range. In fact, in reality there is not even a well-defined hopping range, but rather a distance-dependent electron-hopping rate. Using a distance-dependent electron-hopping rate would allow us to introduce time as a variable in our calculation and to predict an apparent diffusion coefficient instead of reporting percolation thresholds. However, introducing a distance-dependent electron-hopping rate will greatly increase the complexity of our model; thus, given the nature of the approximations involved, we decided to keep our model as simple as possible.

Our model also neglects physical diffusion of viologens, which seems a reasonable assumption given the fact that we observed stable cyclic voltammograms and, therefore, viologens must be strongly adsorbed onto the surfaces of the pores. Another aspect neglected by our model is the existence of dimers within the pores. The UV-vis spectra of the chemically reduced samples (see above) have a band around 550 nm, which is indicative of dimer formation;[44] however it is not clear whether or not the dimers will exist in the unreduced samples. The presence of dimers would reduce the effective surface density of electrochemically active sites thus supporting the conclusion that the low fraction of these sites addressable from the electrode is due to charge-percolation limitations.

In our analysis of the predictions of the RSA/CP model, we focus on the BV-modified pore. The application of RSA/CP to the oligoviologens involves further approximations: PXV shows values of Γ_{abs}^{real} (surface density in terms of real area determined by UV-vis, see Table 3) which are above the percolation threshold (and also above the maximum RSA surface density) calculated for molecular (*i.e.* non-polymeric) redox sites. However, the connectivity of the viologen sites in PXV should increase the theoretical percolation threshold. On the other hand, the role of segmental motions, which are known to assist charge transport,[57] should be much more relevant for the viologen oligomers than for BV.

In summary, our calculation with the RSA/CP model serves as a very first theoretical exploration of charge transport for pore-confined redox molecules. Despite the approximations involved, we believe that the fact that the theoretically predicted surface density at the percolation threshold is of the same order of magnitude as the experimental surface densities supports the idea that the low fraction of electrochemically addressable viologens is due to inefficient electron-hopping. It is worthwhile to note that the validity of this conclusion is not too sensitive to the choice of the model parameters: the percolation thresholds for very different sets of parameters (which we showed in Fig. 8) vary in the range 0.1–0.5 nm^2, which spans less than an order of magnitude.

Conclusions

In this work, we studied the preparation of hybrid viologen/mesoporous silica materials using the infiltration route. Our preliminary experiments showed that high-molecular-weight polymers were unable to infiltrate the mesopores and, hence, we decided to prepare and explore the infiltration of low-molecular weight viologen oligomers. We observed efficient adsorption of these oligomers onto the inner walls of the pores. The as-prepared films constitute one of the first examples of redox-active polyelectrolyte/mesoporous silica hybrids. The films show very high electrocatalytic activity toward oxygen reduction, to the point that we were unable to completely remove the catalytic redox peak by thorough bubbling with Ar. We expect to address the electrocatalytic properties of the films in future work.

Interestingly, comparison of viologen surface coverages Q13 obtained by cyclic voltammetry and UV-vis of chemically reduced samples indicates that only around 4–15% of the total viologen sites within our mesoporous films are electrochemically addressable by the electrode during slow-scan-rate (50 mV s^{-1}) CV experiments (a comparison of cyclic voltammetry and

ellipsometry yields an even smaller fraction of 1–4%). This result suggests inefficient charge transport within the film. This conclusion is supported by EIS experiments and digital simulations of cyclic voltammograms that suggest an apparent diffusion coefficient for charge transport $D_{app} < 1.2 \times 10^{-12}$ cm^2 s^{-1}, which is much smaller than those typically observed for redox-polyelectrolyte modified electrodes. To analyze possible limitations to the electron-hopping mechanism, we proposed a random sequential adsorption/charge percolation model, which shows that the minimum surface densities required to efficiently transport charge across the film are of the order of 0.1–0.5 molecules per nm^2. These values are very close to the maximum surface density discussed above and to our experimental results, which supports the idea that inefficient charge percolation (on the timescale of the electrochemical measurement) can lead to the observed small fraction of electrochemically addressable viologens. Our model suggests that inefficient charge transport in viologen-infiltrated mesoporous films is due to the two-dimensional nature of charge propagation by electron-hopping in these systems, which results from the fact that viologens are constrained to a surface (the inner surface of the pores). This situation differs from charge percolation in polymer films, where the redox sites are homogeneously distributed within the film and, therefore, charge propagation occurs in three spatial dimensions.

Inefficient charge transport limits possible applications of our viologen-modified silica-based hybrid materials for electrochromic applications or electrocatalysis. Audebert *et al.* have shown that post-grafting a ferrocene silane to a mesoporous silica film leads to very efficient diffusional charge transport through the film.[19] Interestingly, the redox molecule used by Audebert *et al.* possesses a flexible seven-atom linker between the silane and the ferrocene, whose segmental motions can increase the probability of electron-transfer events. Other work has relied on the use of mesoporous semiconductor matrices such as titania, in order to improve the electronic communication between the redox centers and the electrode.[60] We believe that it may be possible to use these strategies in the future to overcome the limitations of the infiltration route reported here.

Experimental methods

Materials

All regents were analytical grade or higher and were used as received.

Synthesis of poly(*p*-xylyl viologen), PXV, and poly(hexyl viologen), PHV. Oligomeric poly(viologens) were prepared according to procedures in the literature.[61] We reacted 2.5 mmol of 4,4′-bipiridine with either 2.5 mmol of *p*-dibromoxylene (synthesis of PXV) or 2.5 mmol of 1,6-dibromohexane (synthesis of PHV) in 25 ml of dry acetonitrile for 3 days. The resulting solid was filtered and dried. The product was dissolved in water and dialyzed against deionized water for one week. The identity, purity and degree of polymerization of the final product were analyzed by ^{1}H NMR in D_2O solution (see the ESI†).

Synthesis of mesoporous thin films. Mesoporous silica was deposited on indium-tin oxide (ITO) on glass substrates (Delta Technologies, R = 4–8 Ω) for electrochemistry and UV-vis experiments or on silicon substrates for ellipsometry, contact-angle and SEM measurements. The substrates were rinsed with acetone, ethanol and deionized water, dried with nitrogen and modified by dip-coating into a solution of the silica precursor (weight composition: 16% TEOS, 3% F127, 74% ethanol, 7% HCl 0.055 M; mole composition: TEOS : F127 : EtOH : HCl : H_2O = 1 : 3 × 10^{-3} : 21 : 5 × 10^{-3} : 5) at 25 °C, 40% relative humidity and a withdrawing rate of 2 mm s^{-1}. We maintained the as-prepared films in a 50% relative humidity chamber for one hour and then we removed the organic components of the film using a three-step calcination protocol (1 h at 60 °C, followed by 1 h at 130 °C and finally 2 h at 300 °C). We allowed the films to cool to room temperature, rinsed them with ethanol and dried with nitrogen.

Infiltration with viologens

We immersed the mesoporous films in 20 mM solutions of PXV, PHV or benzyl viologen (BV) for 1 hour (this time was determined in preliminary experiments and was enough to observe saturation of the amount of adsorbed polymer), thoroughly rinsed them with deionized water and dried under nitrogen flow. Long immersion times and alkaline solutions should be avoided in order to prevent dissolution of the silica film. Unless specified, the infiltration solutions contained no added salt and had pH ∼ 5.

Electrochemistry. Electrochemical measurements were performed in a three-electrode electrochemical cell using a Ag/AgCl (3 M KCl) reference electrode and a Pt-mesh counter electrode. The Teflon cell exposed an area of 0.25 cm^2 of the working electrode to the solution (KNO_3 50 mM) using an inert o-ring. Cyclic voltammetry and EIS were performed under an Ar atmosphere with an Autolab potentiostat (Eco-Chemie, Utrecht). EIS analysis was performed with the software Z-View (Scribner Associates).

Ellipsoporosimetry. We used a SOPRA GES5A spectroscopic ellipsometer to determine the ellipsometric quantities $\psi(\lambda)$ and $\Delta(\lambda)$ for λ = 275–830 nm. We first fitted $\psi(\lambda)$ and $\Delta(\lambda)$ for the bare silicon substrate to obtain the wavelength-dependent refractive index – $n(\lambda)$ – and extinction coefficient – $k(\lambda)$ – of the substrate, which were fixed in subsequent fittings. A one-layer Cauchy model, which approximates the mesoporous film by a homogeneous film with an effective refractive index n_{eff}, provided a good fit to the ellipsometric angles for the film/substrate system. Unless otherwise stated, refractive indices used in this work are those at λ = 633 nm. From the fit, we obtained n_{eff} and the thickness of the film (we set k = 0 for the film). We controlled the relative humidity in the ellipsometric experiments using a nitrogen flux containing a controlled content of water vapor. Pore size distributions (Fig. 2c) were obtained from the analysis of the refractive index variation as a function of the water vapor pressure, using the WinElli 2 software (SOPRA, Inc.).

Scanning electron microscopy (SEM)

Images were acquired with a FEG-SEM (Zeiss DSM 982 GEMINI, Carl Zeiss, Oberkochen, Germany) operating at 5 kV.

Chemical reduction/UV-vis experiments. The spectrophotometric quantification of reduced viologen species was performed with a Shimadzu UV-1601 spectrophotometer using mesoporous silica films on ITO-coated glass. We first set the baseline spectrum with the film immersed in water in a 1 cm UV-vis cuvette, then we reduced the viologen species by adding a concentrated $Na_2S_2O_4$ aqueous solution to the cuvette to reach a final reductant concentration of approximately 10 mM and finally we recorded the spectrum of the reduced sample. We shifted the spectra to set the minimum of absorbance to zero in order to correct for changes in scattering of the solution after the addition of the reductant (these shifts were typically on the order of 0.002 to 0.005 a.u.).

Contact angles

Contact angles were obtained with a KSV CAM 200 contact angle meter using Milli-Q® water.

Conflicts of interest

There are no conflicts to declare.

Acknowledgements

MT and GJAASI are fellows of CONICET. MT and GJAASI acknowledge financial support from Agencia Nacional de Promoción Científica y Tecnológica (ANPCyT, PICT-0099-2015, PICT 0154-2016, PICT 3526-2015, PAE-37063-PME-2006-00038). The Química de Nanomateriales group (CNEA) is thanked for help in ellipsometry measurements.

Notes and references

1 J. Hodak, R. Etchenique, E. J. Calvo, K. Singhal and P. N. Bartlett, *Langmuir*, 1997, **13**, 2708–2716.
2 A. Heller, *Acc. Chem. Res.*, 1990, **23**, 128.
3 M. Vago, M. Tagliazucchi, F. J. Williams and E. J. Calvo, *Chem. Commun.*, 2008, 5746–5748.
4 I. Moriguchi and J. H. Fendler, *Chem. Mater.*, 1998, **10**, 2205–2211.
5 J. Stepp and J. B. Schlenoff, *J. Electrochem. Soc.*, 1997, **144**, L155–L158.
6 D. M. DeLongchamp and P. T. Hammond, *Adv. Funct. Mater.*, 2004, **14**, 224–232.
7 W.-K. Lu, R. L. Elsenbaumer and B. Wessling, *Synth. Met.*, 1995, **71**, 2163–2166.
8 N. Oyama and F. C. Anson, *J. Am. Chem. Soc.*, 1979, **101**, 3450–3456.
9 G. J. Samuels and T. J. Meyer, *J. Am. Chem. Soc.*, 1981, **103**, 307–312.
10 N. Oyama and F. C. Anson, *J. Electrochem. Soc.*, 1980, **127**, 247.
11 F. C. Anson, D. N. Blauch, J.-M. Savéant and C.-F. Shu, *J. Am. Chem. Soc.*, 1991, **113**, 1922–1932.
12 R. J. Mortimer and J. L. Dillingham, *J. Electrochem. Soc.*, 1997, **144**, 1549–1553.
13 A. Walcarius, *Chem. Soc. Rev.*, 2013, **42**, 4098–4140.
14 A. Brunsen, A. Calvo, F. J. Williams, G. J. A. A. Soler-Illia and O. Azzaroni, *Langmuir*, 2011, **27**, 4328–4333.
15 A. Andrieu-Brunsen, S. Micoureau, M. Tagliazucchi, I. Szleifer, O. Azzaroni and G. J. Soler-Illia, *Chem. Mater.*, 2015, **27**, 808–821.
16 J. Redepenning and F. C. Anson, *J. Phys. Chem.*, 1987, **91**, 4549–4553.
17 Y. L. Liu, M. Q. Zhao, D. E. Bergbreiter and R. M. Crooks, *J. Am. Chem. Soc.*, 1997, **119**, 8720–8721.
18 V. Pardo-Yissar, E. Katz, O. Lioubashevski and I. Willner, *Langmuir*, 2001, **17**, 1110–1118.
19 P. Audebert, N. Vilà, C. Allain, F. Maisonneuve, A. Walcarius and P. Hapiot, *ChemElectroChem*, 2015, **2**, 1695–1698.
20 N. Vilà and A. Walcarius, *Electrochim. Acta*, 2015, **179**, 304–314.
21 A. Doménech, M. Alvaro, B. Ferrer and H. García, *J. Phys. Chem. B*, 2003, **107**, 12781–12788.
22 M. Álvaro, B. Ferrer, V. Fornés and H. García, *Chem. Commun.*, 2001, 2546–2547.
23 B. Kumar, K. V. Rao, S. Sampath, S. J. George and M. Eswaramoorthy, *Angew. Chem.*, 2014, **126**, 13289–13293.
24 G. Calzaferri, M. Lanz and J.-W. Li, *Chem. Commun.*, 1995, 1313–1314.
25 T.-W. Hui and M. D. Baker, *J. Phys. Chem. B*, 2001, **105**, 3204–3210.
26 H. A. Gemborys and B. R. Shaw, *J. Electroanal. Chem.*, 1986, **208**, 95–107.
27 B. R. Shaw, K. E. Creasy, C. J. Lanczycki, J. A. Sargeant and M. Tirhado, *J. Electrochem. Soc.*, 1988, **135**, 869–876.
28 E. L. Clennan, *Coord. Chem. Rev.*, 2004, **248**, 477–492.
29 Y. Wang, V. Bansal, A. N. Zelikin and F. Caruso, *Nano Lett.*, 2008, **8**, 1741–1745.
30 Y. Wang and F. Caruso, *Chem. Mater.*, 2006, **18**, 4089–4100.
31 Y. Wang, A. S. Angelatos, D. E. Dunstan and F. Caruso, *Macromolecules*, 2007, **40**, 7594–7600.
32 M. A. Hubbe, N. Wu, O. J. Rojas and S. Park, *Colloids Surf., A*, 2011, **381**, 1–6.
33 J. Elbert, F. Krohm, C. Rüttiger, S. Kienle, H. Didzoleit, B. N. Balzer, T. Hugel, B. Stühn, M. Gallei and A. Brunsen, *Adv. Funct. Mater.*, 2014, **24**, 1591–1601.
34 K. M. Coakley, Y. Liu, M. D. McGehee, K. L. Frindell and G. D. Stucky, *Adv. Funct. Mater.*, 2003, **13**, 301–306.
35 P. C. Angelomé and G. J. d. A. Soler-Illia, *Chem. Mater.*, 2005, **17**, 322–331.
36 A. Calvo, M. C. Fuertes, B. Yameen, F. J. Williams, O. Azzaroni and G. J. A. A. Soler-Illia, *Langmuir*, 2010, **26**, 5559–5567.
37 C. Boissiere, D. Grosso, S. Lepoutre, L. Nicole, A. B. Bruneau and C. Sanchez, *Langmuir*, 2005, **21**, 12362–12371.
38 C. F. Narambuena, D. M. Beltramo and E. P. Leiva, *Macromolecules*, 2007, **40**, 7336–7342.
39 M. Tagliazucchi, D. B. Tice, C. M. Sweeney, A. J. Morris-Cohen and E. A. Weiss, *ACS Nano*, 2011, **5**, 9907–9917.

40 A. Factor and G. E. Heinsohn, *J. Polym. Sci., Part B: Polym. Lett.*, 1971, **9**, 289–295.
41 N. S. Zacharia, D. M. DeLongchamp, M. Modestino and P. T. Hammond, *Macromolecules*, 2007, **40**, 1598–1603.
42 J. Forsman, *Langmuir*, 2012, **28**, 5138–5150.
43 R. E. Sassoon, S. Gershuni and J. Rabani, *J. Phys. Chem.*, 1985, **89**, 1937–1945.
44 S. Mayhew and F. Müller, *Biochem. Soc. Trans.*, 1982, **10**, 176–177.
45 S. E. Creager and M. A. Fox, *J. Electrochem. Soc.*, 1990, **137**, 2151–2157.
46 Q. Lin, Q. Li, C. Batchelor-McAuley and R. G. Compton, *Phys. Chem. Chem. Phys.*, 2013, **15**, 7760–7767.
47 W. H. Koppenol, D. M. Stanbury and P. L. Bounds, *Free Radical Biol. Med.*, 2010, **49**, 317–322.
48 A. J. Bard and L. R. Faulkner, *Electrochemical Methods*, John Wiley and Sons, New York, 2001.
49 M. Tagliazucchi and E. J. Calvo, *ChemPhysChem*, 2010, **11**, 2957–2968.
50 M. E. Tagliazucchi and E. J. Calvo, *J. Electroanal. Chem.*, 2007, **599**, 249–259.
51 M. Tagliazucchi, D. Grumelli and E. J. Calvo, *Phys. Chem. Chem. Phys.*, 2006, **8**, 5086–5095.
52 H. S. White, J. Leddy and A. J. Bard, *J. Am. Chem. Soc.*, 1982, **104**, 4811–4817.
53 M. Sharp and S. Åberg, *J. Electroanal. Chem.*, 1998, **449**, 137–151.
54 J. G. Gaudiello, P. K. Ghosh and A. J. Bard, *J. Am. Chem. Soc.*, 1985, **107**, 3027–3032.
55 C. P. Andrieux and J. M. Saveant, *J. Phys. Chem.*, 1988, **92**, 6761–6767.
56 F. C. Anson, D. N. Blauch, J. M. Saveant and C. F. Shu, *J. Am. Chem. Soc.*, 1991, **113**, 1922–1932.
57 D. N. Blauch and J. M. Saveant, *J. Am. Chem. Soc.*, 1992, **114**, 3323–3332.
58 J. Feder, *J. Theor. Biol.*, 1980, **87**, 237–254.
59 M. Tagliazucchi, F. Zou and E. A. Weiss, *J. Phys. Chem. Lett.*, 2014, **5**, 2775–2780.
60 S. Y. Choi, M. Mamak, N. Coombs, N. Chopra and G. A. Ozin, *Nano Lett.*, 2004, **4**, 1231–1235.
61 A. Factor and G. Heinsohn, *J. Polym. Sci., Part B: Polym. Lett.*, 1971, **9**, 289–295.

